RESEARCH ARTICLES

Preliminary studies on different modes of interaction between hemorrhagic and non-hemorrhagic p-i snake venom metalloproteinases with basement membrane substrates: insights from an *In silico* approach

Authors

Jaime Andrés Pereañez[1,*], Arley Camilo Patiño[1], José María Gutiérrez[2], Lina María Preciado[1]

Affiliations

1. Programa de Ofidismo/Escorpionismo, Departamento de Farmacia, Facultad de Ciencias Farmacéuticas y Alimentarias, Universidad de Antioquia UdeA, Calle 70 No. 52-21, Medellín, Colombia.

2. Instituto Clodomiro Picado, Facultad de Microbiología, Universidad de Costa Rica, San José, Costa Rica.

***Corresponding author:**

Jaime Andrés Pereañez, Programa de Ofidismo/Escorpionismo, Departamento de Farmacia, Facultad de Ciencias Farmacéuticas y Alimentarias, Universidad de Antioquia UdeA, Calle 70 No. 52-21, Medellín, Colombia. Phone: 57-4-2196649; FAX: 57-4-2631914; E mail: andrespj20@gmail.com

Abstract

It has been demonstrated that, in vivo, a hemorrhagic P-I SVMP hydrolyzes type IV collagen and perlecan to a higher extent than a non-hemorrhagic P-I SVMP. In order to gain further insights on this phenomenon, the protein-protein docking approach was used to analyze the mode of interaction of four different SVMPs with two different domains of perlecan and two different domains of type IV collagen. The hemorrhagic SVMPs are BaP1 and acutolysin-A, and the non-hemorrhagic ones are BmooMPα-I and H2-proteinase. In general, hemorrhagic SVMPs could form catalytic complexes with the triple-helical domain of type IV collagen, and with laminin-like globular domain 3 and immunoglobulin (IG)-like domain of perlecan. It is hypothesized that the formation of these catalytic complexes may explain the differences observed in vivo in the degradation of collagen IV and perlecan. Moreover, our results suggest that there are differences in the area and volume of the active site cleft between hemorrhagic and non-hemorrhagic P-I SVMPs, since the latter present a larger volume and area. We suggest that this structural characteristic favors the interaction with substrates; nevertheless, at the same time, it could decrease the probability to achieve a stable complex. However, these results should be confirmed by means of experimental and bioinformatics assays.

Key words: Snake venom metalloproteinases, protein-protein docking, collagen type IV, perlecan, hemorrhage.

1. Introduction

Snake venom metalloproteinases (SVMPs) are abundant in viperid snake venoms[1], and belong to the reprolysin subgroup of metalloproteinases[2]. SVMPS participate in the pathogenesis of viperid snakebite envenoming by inducing local and systemic hemorrhage, blistering, dermonecrosis, myonecrosis, and defibrinogenation[3]. SVMPs induce hemorrhage by proteolytic degradation of extracellular matrix components of the basement membrane (BM) of the microvasculature, which is involved in the maintenance of capillary structure and integrity[2, 4-6]. SVMPs have been classified in four main groups on the basis of their different domain constitution, as follows: P-I (SVMPs comprised by single metalloproteinase domain), P-IIa to P-IIe (containing metalloproteinase and disintegrin domains), P-IIIa to P-IIIc (containing metalloproteinase, disintegrin-like and cysteine-rich domains), and P-IIId, formerly known as P-IV (containing the P-III structure and two C-type lectin-like domains connected by disulfide bonds to the cysteine-rich domain)[7].

SVMPs of the P-I group differ significantly in their ability to induce hemorrhage[5, 8-12]. Despite having similar proteolytic activity towards several substrates *in vitro*, some of these enzymes are hemorrhagic whereas others are not[9, 11, 13]. Several attempts have been made to clarify these differences from the structural standpoint[14-16]. Nevertheless, the detailed structural determinants of hemorrhagic activity of P-I SVMPs remain largely unknown, and the possibility to predict the hemorrhagic potential of SVMPs on the basis of structure or sequence analysis remains uncertain, although a recent hypothesis proposed that differences in the dynamics of a loop located near the catalytic site might explain the variable hemorrhagic activity[15].

Escalante et al.[13] described important differences between hemorrhagic and non-hemorrhagic SVMPs in their ability to hydrolyze BM components *in vivo*. BaP1, a hemorrhagic P-I SVMP, hydrolyzes type IV collagen and perlecan to a higher extent than Leucurolysin-A, a non-hemorrhagic P-I SVMP. In addition, the proteomic analysis of exudates collected from muscle tissue injected with these SVMPs also revealed differences in the types of extracellular matrix components present[13].

We presume that the mode of interaction of SVMPs with BM substrates is critical for their ability to hydrolyze them and, consequently, to disrupt the integrity of the microvessel wall. However, because no structures of protein-protein complexes of SVMPs and BM components are available, the characterization of such structural features remains elusive. In order to gain insights for understanding the biological differences of P-I SVMPs, in this study we used the protein-protein docking approach to analyze the mode of interaction of four different SVMPs with two different domains of perlecan and two different domains of type IV collagen. To perform this comparative analysis, we selected two hemorrhagic and two non-hemorrhagic SVMPs. Our *in silico* approach allowed the identification of structural features that may determine differences in the interaction between SVMPs and these substrates, thus providing information that might explain their variable hemorrhagic potential and thus provide information for the design of novel experimental approaches to address this issue.

2. Materials and methods

2.1. Structures

The structures of SVMPs BaP1 (1ND1) (hemorrhagic), Acutolysin A (1BUD) (hemorrhagic), H2-proteinase (1WNI) (non-hemorrhagic), and BmooMPα-I (3GBO) (non-hemorrhagic), and the structures of the noncollagenous (NC1) domain of human placenta type IV collagen (1LI1), the synthetic triple-helical structure of collagen (containing the classical Gly-X-Y sequence motif), used to simulate the helical domain of type IV collagen (1BKV), and the laminin-like globular domain 3 (LG3) of human perlecan (3SH4) were downloaded from PDB (http://www.rcsb.org/pdb/home/home.do). The structure of human third immunoglobulin (IG)-like domain of perlecan (IG3) was modeled from the IG3 structure from *Mus musculus* (PDBD: 1GL4:B). The protein with known structure has 91.84 % identity with the segment between residues 1761 and 1859 of human perlecan (UniProtKB code P98160). The model was built using EasyModeller[17], a graphical user interface for the program Modeller (9v8)[18]. This program is completely automated and is capable of generating energy minimized protein models by satisfying spatial restraints on bond distances and dihedral angles extracted from the template PDB file. Modeller performs an automatic loop modeling and model optimization. The stereochemical excellence of model and the overall structural geometry were confirmed by Procheck program[19]. The Verify 3D program was used to determine the compatibility of an atomic model (3D) with its own amino acid sequence (1D) by assigning a structural class on the basis of its location and environment (alpha, beta, loop, polar, non-polar, etc.) as well as by comparing the results with good database structures[20]. The energy of residues was checked by ProSA, using the web service ProSA-web[21, 22].

2.2. Protein structure preparation

The structure of the proteins was prepared using the Protein Preparation module implemented in the Maestro program. For SVMPs the catalytic water was identified and kept during the docking process. Then, hydrogen atoms were automatically added to each protein according to the chemical nature of each amino acid, on the basis of the ionized form expected in physiological condition. This module also controls the atomic charges assignment. Finally, each 3D structure of the protein was relaxed through constrained local minimization, using the OPLS force fields in order to remove possible structural mismatches due to the automatic procedure employed to add the hydrogen atoms. When necessary, bonds, bond orders, hybridizations, and hydrogen atoms were added, and charges were assigned (a formal charge of +2 for Zn ion for SVMPs).

2.3. Protein-protein docking

The rigid-body molecular docking procedure was performed using the program PatchDock[23]. For this process, the SVMPs were chosen as receptors, while NC1 domain, triple-helical collagen, and IG3 and LG3 perlecan domains were selected as ligands. Then, the PatchDock solutions were submitted to a refinement process, using the tool FiberDock[24, 25]. PatchDock is a geometry-based molecular docking algorithm. It is aimed at finding docking transformations that yield good molecular shape complementarity. Such transformations, when applied, induce both wide interface areas and small amounts of steric clashes. A wide interface is ensured to include several matched local features of the docked molecules that have complementary characteristics. The PatchDock algorithm

divides the surface representation of the molecules into concave, convex and flat patches. Then, complementary patches are matched in order to generate candidate transformations. Each candidate transformation is further evaluated by a scoring function that considers both geometric fit and atomic desolvation[23]. On the other hand, FiberDock models both side-chain and backbone flexibility and performs rigid-body optimization on the ligand orientation. The backbone and side-chain movements are modeled according to the Van der Waals forces between the receptor and ligand. Finally, FiberDock ranks the refined solutions by a binding energy scoring function. This score includes Atomic Contact Energy, softened van der Waals interactions, partial electrostatics, and additional estimations of the binding free energy[24, 25]. After Fiberdock refinement, the solution with the highest global energy (binding energy) was chosen.

2.4. Pocket information

The CASTp server (using the default settings) was used for the identification of the main binding site in SVMPs[26]. CASTp provides identification and analytical measurements of surface accessible pockets, for proteins and other molecules, which can be used to guide protein–protein interactions. In order to assess whether the differences between the mean values of volumes and areas of the main cavity were significant, a nonparametric t test was applied (Unpaired t test with Welch´s correction).

3. Results

3.1. Interaction of SVMPs with NC1 domain and triple-helical region of type IV collagen

Protein-protein docking between hemorrhagic P-I SVMPs and triple-helical collagen suggested that enzymes could bind type IV collagen and could form a catalytic complex, in which a Leu residue is located in the active site cleft of SVMPs (Fig. 1A and 1B; Fig. 1A and1B, Supplementary material). In contrast, docking between non-hemorrhagic P-I SVMPs and triple-helical collagen evidenced that these enzymes could interact with collagen, but could not form a catalytic complex (Fig. 1C and 1D; Fig. 1C and 1D, Supplementary material). In these complexes the substrate-binding pocket of the enzymes was empty. On the other hand, generated complexes between NC1 domain of type IV collagen and SVMPs showed that the four SVMPs could not form catalytic complexes with this domain (Fig. 2A and 2B).

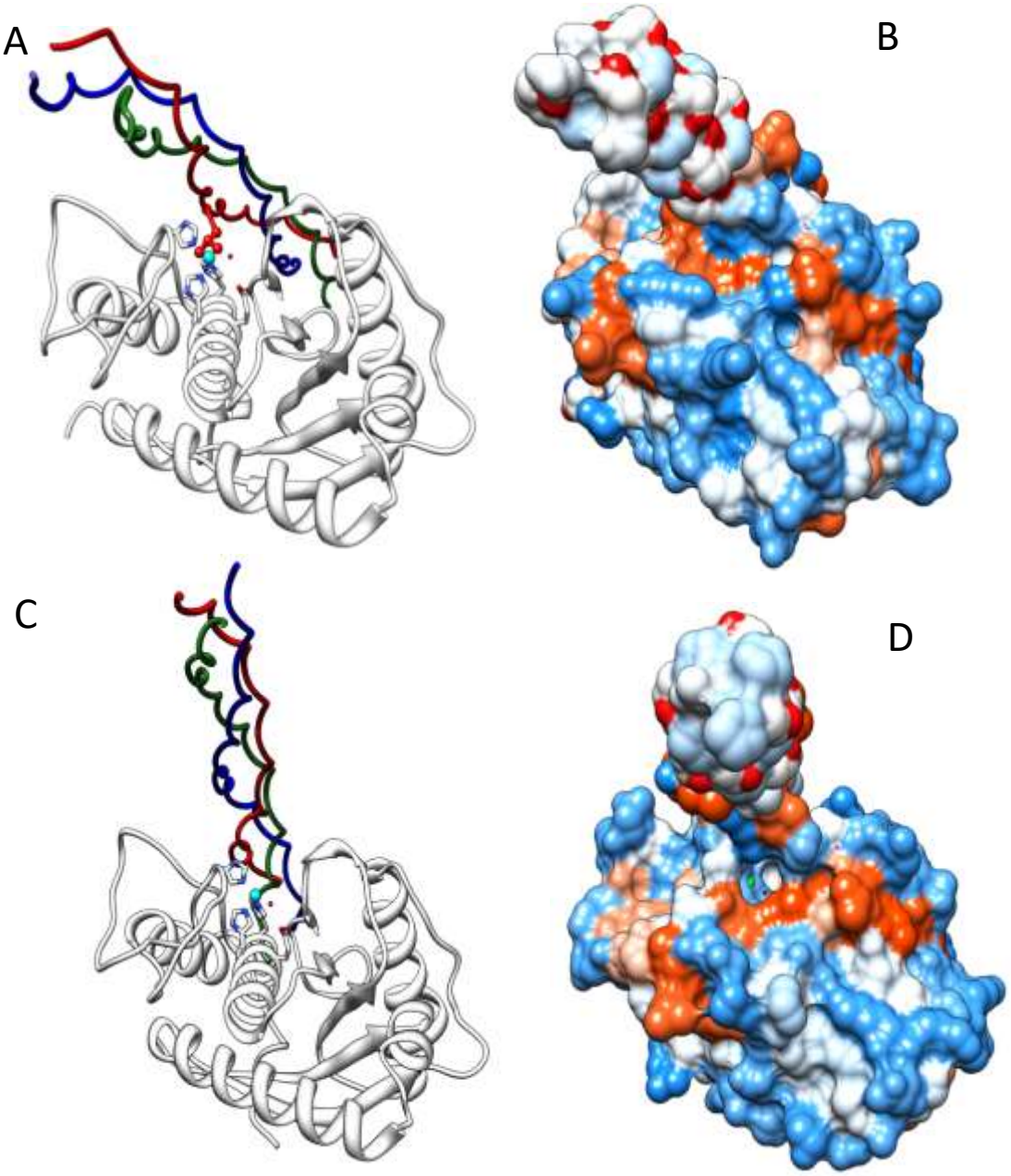

Figure 1. Interaction of hemorrhagic and non-hemorrhagic P-I SVMP and triple-helical region of collagen. **A.** Ribbon representation of the interaction of BaP1 with triple-helical collagen. **B.** Hydrophobicity-surface representation of the interaction between BaP1 and triple-helical collagen. **C.** Ribbon representation of the interaction of BmooMPα-I with triple-helical collagen. **D.** Hydrophobicity-surface representation of the interaction between BmooMPα-I and triple-helical collagen. In **A** and **C** the catalytic water and the active site of SVMPs is displayed in sticks, and Zn^{2+} ion is colored in cyan. The chains A, B and C of collagen are colored in red, green and blue, respectively. In **A**, the Leu residue occupying the active site cleft of SVMPs is shown in balls and sticks. Note in **B** that the active site is filled by collagen chains, whereas in **D** the active site is not occupied by these chains.

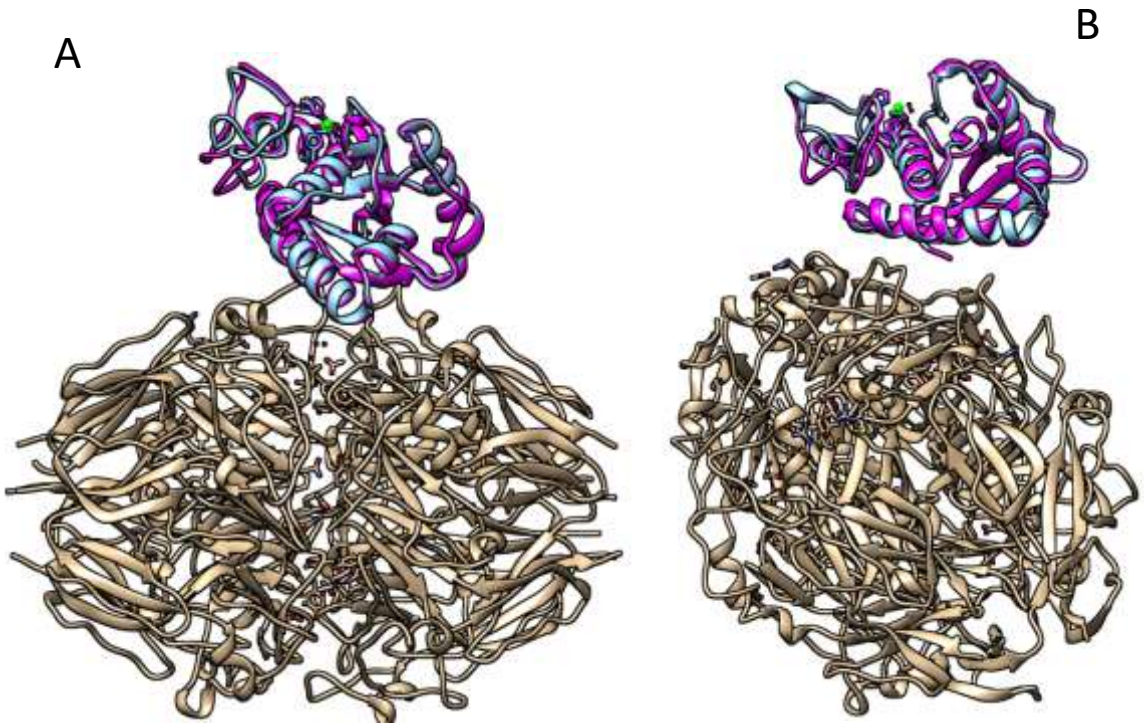

Figure 2. Interaction of P-I SVMPs with NC1 domain of type IV collagen. **A.** Interaction of hemorrhagic P-I SVMPs with NC1 domain of type IV collagen. BaP1 is displayed in magenta, while Acutolysin A is shown in cyan. **B.** Interaction of non-hemorrhagic P-I SVMPs with NC1 domain of type IV collagen. BmooMPα-I is colored in magenta, whereas H2-proteinase is presented in cyan. In both cases, Zn^{2+} ion is shown as a green sphere.

3.2. Interaction of SVMPs with IG3 and LG3 domains of perlecan

The quality of the homology model of IG3 domain of perlecan was evaluated by Procheck; the detailed residue-by-residue stereochemical quality of the IG3 model was found to be good (94.9% in most favored regions, 5.1% in additional allowed regions and 0% in generously allowed regions and disallowed regions) (Fig. 2, Supplementary material). The Verify 3D program was used to determine the compatibility of an atomic model (3D) with its own amino acid sequence (1D). The scores were between 0.00 and 0.48 (Fig. 3, Supplementary material). The energetic architecture of protein folds was determined by using the program ProSA. This analysis of the model revealed a Z-score value of -5.35, which is in the range of native conformations of the template (0.00) (Data not shown). The energy profile of the IG3-domain predicted model was found to be good (Fig. 4, Supplementary material). This model showed that most of the residues are in the negative region.

Protein-protein docking between hemorrhagic P-I SVMPs and IG3-domain of perlecan suggested that enzymes could bind this domain and then could form a catalytic complex, in which a Leu residue is located in the active site cleft of the proteinase (Fig. 3A and 4B; Fig. 5A and 5B, Supplementary material). Conversely, docking between non-hemorrhagic P-I SVMPs and IG3 domain of perlecan evidenced that,

although these enzymes could interact in different forms with this domain of perlecan, they could not form a catalytic complex (Fig. 3C and 3D; Fig. 5C and 5D, Supplementary material). In these complexes, the substrate-binding pocket of the enzymes was unoccupied.

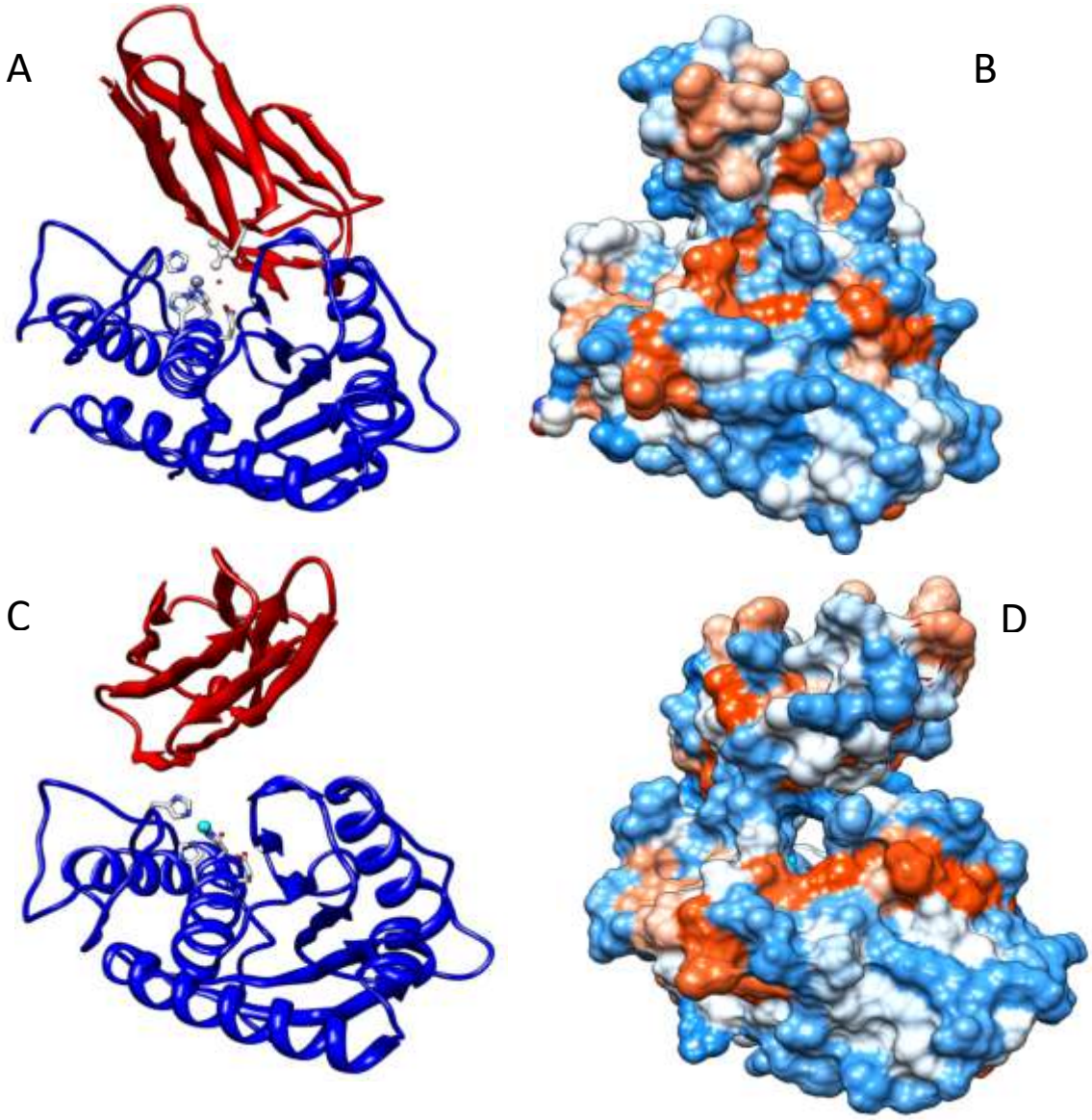

Figure 3. Docking results between hemorrhagic and non-hemorrhagic P-I SVMPs and IG3-domain of perlecan. **A.** Ribbon representation of the interaction of BaP1 with IG3-domain of perlecan. **B.** Hydrophobicity-surface representation of the interaction between BaP1 and IG3-domain of perlecan. **C.** Ribbon representation of the interaction of BmooMPα-I with IG3-domain of perlecan. **D.** Hydrophobicity-surface representation of the interaction between BmooMPα-I and IG3-domain of perlecan. In **A** and **C**, the catalytic water and the active site of SVMPs are displayed in sticks, and Zn^{2+} ion is colored in cyan. SVMPs and IG3-domain of perlecan are colored in blue and red, respectively. In **A**, the Leu residue occupying the active site cleft of SVMPs is shown in balls and sticks. Note in **B** that the substrate binding pocket is occupied by IG3-domain of perlecan, whereas in **D** the substrate binding pocket is unfilled.

The generated complexes between LG3 of perlecan and hemorrhagic P-I SVMPs suggested that these enzymes could bind this domain and form a catalytic complex, in which a Pro residue is located in the active site cleft of SVMPs (Fig. 4A and 4B). In contrast, docking between non-hemorrhagic P-I SVMPs and LG3 domain of perlecan indicated that, although these enzymes could interact with this domain of perlecan, they cannot form a catalytic complex (Fig. 4C and 4D).

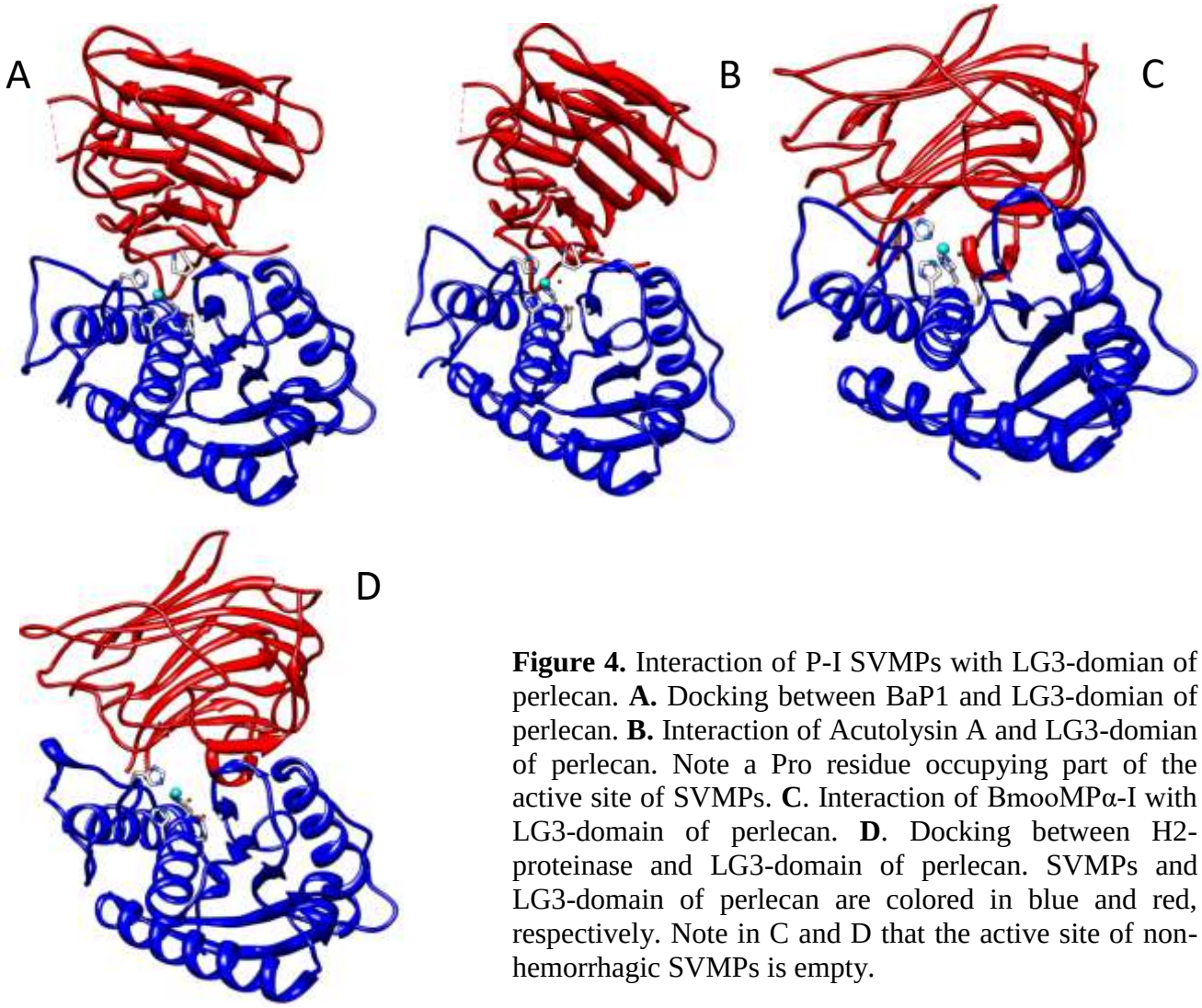

Figure 4. Interaction of P-I SVMPs with LG3-domian of perlecan. **A.** Docking between BaP1 and LG3-domian of perlecan. **B.** Interaction of Acutolysin A and LG3-domian of perlecan. Note a Pro residue occupying part of the active site of SVMPs. **C**. Interaction of BmooMPα-I with LG3-domain of perlecan. **D**. Docking between H2-proteinase and LG3-domain of perlecan. SVMPs and LG3-domain of perlecan are colored in blue and red, respectively. Note in C and D that the active site of non-hemorrhagic SVMPs is empty.

3.3. Pocket information

CAStp sever identified 25, 18, 27 and 19 cavities for BaP1, Acutolysin A, H_2-proteinase and BmooMPα-I, respectively. Nevertheless, the main cavity was that corresponding to the active site cleft. The volumes ($Å^3$) of this cavity were 237.0, 214.5, 311.4 and 339.6 and the areas ($Å^2$) were 190, 165, 261 and 243 for BaP1, Acutolysin A, H_2-proteinase and BmooMPα-I, respectively. Statistically

significant differences between volumes (p=0.0312) and areas (p=0.0402) between hemorrhagic and non-hemorrhagic SVMPs were obtained.

4. Discussion

SVMPs play key roles in envenomings by snakes of the family Viperidae (3). One of the most notorious functional properties of these enzymes is their ability to disrupt microvessels, provoking local and systemic hemorrhage[3,4]. SVMPs share a highly similar structure in their catalytic domain; however, they greatly differ in their ability to induce hemorrhage[4]. In general, P-III SVMPs are more potent hemorrhagic toxins than P-I SVMPs. This is likely to depend on the presence, in the former, of extra domains in addition to the catalytic one, since exosites in disintegrin-like and cysteine-rich domains enable these enzymes to bind to relevant targets in the extracellular matrix or in endothelial cells[27-30]. On the other hand, significant variations in hemorrhagic activity occur also within the P-I SVMPs[8, 9, 11, 13]. The structural basis of such variable hemorrhagic profile remains largely unknown.

In a recent work, Escalante et al.[13] evidenced differences between hemorrhagic and non-hemorrhagic SVMPs in their capacity to degrade BM components *in vivo*. A hemorrhagic P-I SVMP hydrolyzes collagen type IV and perlecan to a greater extent than a non-hemorrhagic P-I SVMP, thus suggesting that differences in the ability of SVMPs to hydrolyze these structurally-relevant components of the BM may explain their variable hemorrhagic potency. Therefore, we assessed the mode of interaction of hemorrhagic and non-hemorrhagic SVMPs with three-dimensional structures of several domains of these BM proteins.

All type IV collagens in mammals are derived from six genetically distinct α-chain polypeptides (α_1–α_6)[31]. The type IV collagen α-chains have similar domain structures and share between 50–70% identity at the amino acid sequence level[31]. The α-chains present three domains: an amino-terminal 7S domain, a middle triple-helical domain, and a carboxy-terminal globular non-collagenous (NC)-1 domain. The triple-helical part is the longest domain, of about 1,400 amino acids in length, with around 22 interruptions within the classical Gly-X-Y sequence motif characteristic of collagens. The NC1 domain of each α-chain is about 230 residues in length[31].

On the other hand, perlecan (also known as basement membrane-specific heparan sulfate proteoglycan core protein) is a core protein of molecular mass 470 KDa to which three long chains of glycosaminoglycans are bound[32, 33]. Perlecan has five (I-V) structural domains. Domain I contains attachment sites for heparan sulfate. Domain II contains four repeats that are similar to the low density lipoprotein (LDL) receptor class A, followed by an immunoglobulin (Ig)-like repeat. Domain III has three globular domains that are homologous to the laminin domain IV, and that are flanked and interrupted by nine laminin–EGF (epidermal growth factor)-like repeats. Domain IV contains 21 Ig-like repeats that have homology to the neural cell-adhesion protein N-CAM. Finally, domain V/endorepellin contains three globular domains that have homology to laminin G domains and are each separated by two sets of EGF-like repeats[32, 33].

To simulate the largest domain (triple-helical domain) of type IV collagen, we used an available structure of collagen that has Gly-X-Y

sequence motif. Docking results suggested that hemorrhagic P-I SVMPs could form a catalytic complex with this domain. In addition, these analyses evidenced that a Leu residue is likely to occupy part of the active site of hemorrhagic P-I SVMPs. This Leu is in the P1´ site of the substrate. Similar findings were obtained with hemorrhagic PI-SVMPs and the IG3-domain of perlecan. These observations are in agreement with a recent study in which hemorrhagic P-I SVMPs displayed preference for a Leu residue in the P1´site[34]. In addition, our results agree with the crystal structure of the catalytic complex between a matrix metalloproteinase and a collagen fiber, in which a Leu residue in the P1´site of the substrate is interacting with the active site clef of the enzyme (35). In contrast, our findings suggest that neither hemorrhagic nor non-hemorrhagic SVMPs are likely to form a catalytic complex with the NC1 domain of type IV collagen. These results agree with those of Baramova et al.[36], who reported that Ht-e, a P-I SVMPs isolated from the venom of the rattlesnake *Crotalus atrox*, does not exert proteolytic activity towards the hexameric globular NC1 domains of type IV collagen. This is likely due to the fact that the NC1 domain does not have solvent-exposed regions that could interact with the substrate-binding cleft of SVMPs. Moreover, the NC1 domain has several intermolecular disulfide bonds which contribute to the compact structure of this globular domain[37]. On the other hand, docking between LG3 domain of perlecan and hemorrhagic P-I SVMPs suggests that the substrate binding pocket would be occupied by a Pro residue. Nevertheless, proline was reported as a negative selection for positions P1´and P2´ for hemorrhagic SVMPs[34].

Interaction and further formation of catalytic complexes between hemorrhagic P-I SVMPs with triple-helical domain of type IV collagen could explain the higher degradation of this substrate by these toxins as compared to non-hemorrhagic P-I SVMPs. This hydrolytic activity on type IV collagen has been proposed to be a key step to destabilize the capillary scaffold, because it confers structural stability to the BM, enabling it to resist mechanical stress[31, 38]. In the same way, catalytic complexes between hemorrhagic P-I SVMPs and IG3/LG3 domains of perlecan could explain the described degradation of this BM substrate *in vivo*[13]. The hydrolysis of these enzymes on perlecan could contribute to the destabilization of BM, as perlecan plays a key role in the integration of laminin and type IV collagen and in linking the various components of the BM[32, 33]. Moreover, perlecan is known to contribute to the resistance of BM to mechanical stress[32, 33].

Our docking studies revealed possible interactions and formation of catalytic complexes between P-I SVMPs, especially hemorrhagic ones, and several domains of type IV collagen and perlecan. Nevertheless, there might be other regions of these complex molecules, not tested in our *in silico* approach, which may also interact with SVMPs. For example, Baramova et al.[36] reported that Ht-e, a P-I SVMP, hydrolyzes *in vitro* the α1 (IV) chains of type IV collagen at position Ala258-Gln259, in a region where the triple helix is interrupted. Thus, hemorrhagic P-I SVMPs are likely to hydrolyze BM substrates also in domains different from those discussed in our analysis. Further studies should be performed on the molecular interactions between SVMPs and BM components.

In an effort to identify structural determinants involved in the hemorrhagic activity induced by SVMPs, Ramos and Selistre-de-Araujo[14] reported a slight, but linear, correlation of the characteristics of a polar molecular surface area and the hemorrhagic potential. In addition, structural analysis of several hemorrhagic and non-hemorrhagic SVMPs revealed small variations in a loop (from residue 156 to 175) region surrounding the active site cleft[16]. More recently, Wallnoefer et al.[15] used molecular dynamics and reported that hemorrhagic active P-I SVMPs exhibit a significantly higher flexibility in the first part of the loop (before the Met-turn; residues 156-163), while the inactive ones have much higher flexibility in the loop region after the Met-turn (residue numbers 166-175). Our results evidenced statistically significant differences between the volumes and areas of the active site pocket between hemorrhagic and non-hemorrhagic SVMPs, since the latter have larger volume and area. We presume that this structural characteristic could favor the interaction with substrates; however, this may also decrease the probability to achieve a stable catalytic complex. Additionally, we hypothesize that the movement of the first part of the loop in the hemorrhagic SVMPs could also provoke movements in the zinc-coordination motif, which may also bring this motif and the catalytic water closer to the substrate, also resulting in a reduction of the volume of the active site cleft. On the other hand, movements of the second part of the loop in the inactive hemorrhagic SVMPs could change the shape and increase the volume of the substrate binding pocket (Fig. 6, Supplementary material). To summarize, the movements of the loop 156-175 might influence the catalytic activity of the SVMPs. These shakes could change the shape of the active site and, hence, might influence the way by which SVMPs interact with BM substrates, a hypothesis that requires further studies. The co-crystallization of hemorrhagic and non-hemorrhagic SVMPs with their substrates will provide key structural features to further understand the basis of the different ability of P-I SVMPs to induce hemorrhage.

CONCLUSIONS

Our results suggest that hemorrhagic and non-hemorrhagic SVMPs interact in different ways with the BM substrates type IV collagen and perlecan. In general, hemorrhagic SVMPs could form catalytic complexes with the triple-helical domain of type IV collagen, and with IG3 and LG3 domains of perlecan. The formation of these catalytic complexes might explain the differences previously described on the hydrolysis of type IV collagen and perlecan *in vivo*. Moreover, our results suggest that there are differences in the area and volume of the active site cleft between hemorrhagic and non-hemorrhagic SVMPs. It is hypothesized that the dynamics of the loop located nearby the active site may influence the shape and volume of the substrate binding pocket, with the consequent impact on catalytic activity. However, these results should be confirmed by means of experimental and bioinformatics assays.

ACKNOWLEDGEMENTS

The authors acknowledge Universidad de Antioquia (UdeA and Project CIQF-217) and Vicerrectoría de Investigación (Universidad de Costa Rica)

REFERENCES

1. Calvete JJ. Proteomic tools against the neglected pathology of snake bite envenoming. Exp. Rev. Proteomics. 2011; 8: 739-758.
2. Fox JW, Serrano SMT. Structural considerations of the snake venom metalloproteinases, key members of the M12 reprolysin family of metalloproteinases. Toxicon. 2005; 45: 969-985.
3. Gutiérrez JM, Rucavado A, Escalante T. Snake venom metalloproteinases. Biological roles and participation in the pathophysiology of envenomation. In Mackessy SP, ed., Handbook of Venoms and Toxins of Reptiles. Boca Raton: CRC Press; 2010. pp 114-128.
4. Gutiérrez JM, Rucavado A, Escalante T, Díaz C. Hemorrhage induced by snake venom metalloproteinases: biochemical and biophysical mechanisms involved in microvessel damage. Toxicon. 2005; 45: 997-1011.
5. Escalante T, Rucavado A, Fox JW, Gutiérrez JM. Key events in microvascular damage induced by snake venom hemorrhagic metalloproteinases. J. Proteomics. 2011b; 74: 1781-1794.
6. Escalante T, Shannon J, Moura-da-Silva AM, Gutiérrez JM, Fox JW. Novel insights into capillary vessel basement membrane damage by snake venom hemorrhagic metalloproteinases: a biochemical and immunohistochemical study. Arch. Biochem. Biophys. 2006; 455: 144-153.
7. Fox JW, Serrano SM. Insights into and speculations about snake venom metalloproteinase (SVMP) synthesis, folding and disulfide bond formation and their contribution to venom complexity. FEBS Journal. 2008; 275: 3016-3030.
8. Akao PK, Tonoli CC, Navarro MS, Cintra AC, Neto JR, *et al*. Structural studies of BmooMPalpha-I, a non-hemorrhagic metalloproteinase from *Bothrops moojeni* venom. Toxicon. 2010; 55: 361-368.
9. Bello CA, Hermogenes AL, Magalhaes A, Veiga SS, Gremski LH, *et al*. Isolation and biochemical characterization of a fibrinolytic proteinase from *Bothrops leucurus* (white-tailed jararaca) snake venom. Biochimie. 2006; 88: 189–200.
10. Gong W, Zhu X, Liu S, Teng M, Niu L. Crystal structures of acutolysin A, a three-disulfide hemorrhagic zinc metalloproteinase from the snake venom of *Agkistrodon acutus*. J. Mol. Biol. 1998; 283: 657-668.
11. Gutiérrez JM, Romero M, Díaz C, Borkow G, Ovadia M. Isolation and characterization of a metalloproteinase with weak hemorrhagic activity from the venom of the snake *Bothrops asper* (terciopelo). Toxicon. 1995; 33: 19-29.
12. Kumasaka T, Yamamoto M, Moriyama H, Tanaka N, Sato M, *et al*. Crystal structure of H2-proteinase from the venom of *Trimeresurus flavoviridis*. J. Biochem. 1996; 119: 49-57.
13. Escalante T, Ortiz N, Rucavado A, Sanchez EF, Richardson M, *et al*. Role of collagens and perlecan in microvascular stability: exploring the mechanism of capillary vessel damage by snake venom metalloproteinases. PLoS One. 2011a; 6: e28017.
14. Ramos OH, Selistre-de-Araujo HS. Comparative analysis of the catalytic domain of hemorrhagic and non-hemorrhagic snake venom metallopeptidases using bioinformatic tools. Toxicon. 2004; 44: 529-538.

15. Wallnoefer HG, Lingott T, Gutiérrez JM, Merfort I, Liedl KR. Backbone flexibility controls the activity and specificity of a protein-protein interface: specificity in snake venom metalloproteinases. J. Am. Chem. Soc. 2010; 132: 10330-10337.
16. Watanabe L, Shannon JD, Valente RH, Rucavado A, Alape-Girón A, *et al*. Amino acid sequence and crystal structure of BaP1, a metalloproteinase from *Bothrops asper* snake venom that exerts multiple tissue-damaging activities. Protein Sci. 2003; 12: 2273-2281.
17. Kuntal BK, Aparoy P, Reddanna P. EasyModeller: A graphical interface to MODELLER. BMC Res. 2010; Notes 3: 226.
18. Sali A, Blundell TL. Comparative protein modelling by satisfaction of spatial restraints. J. Mol. Biol. 1993; 234: 779-815.
19. Laskowski RA, MacArthur MW, Moss DS, Hornton DS. PROCHECK: a program to check the stereochemical quality of protein structures. J. Appl. Crystallogr. 1993; 26: 283-291.
20. Bowie JU, Lüthy R, Eisenberg D. A method to identify protein sequences that fold into a known three-dimensional structure. Science. 1991; 253: 164-170.
21. Sippl MJ. Recognition of errors in three-dimensional structures of proteins. Proteins. 1993; 17: 355-362.
22. Wiederstein M, Sippl MJ. ProSA-web: interactive web service for the recognition of errors in three-dimensional structures of proteins. Nucleic Acids Res. 2007; 35: W407-410.
23. Schneidman-Duhovny D, Inbar Y, Nussinov R, Wolfson HJ. PatchDock and SymmDock: servers for rigid and symmetric docking. Nucleic Acids Res. 2005; 33: W363-367.
24. Mashiach E, Nussinov R, Wolfson HJ. FiberDock: Flexible induced-fit backbone refinement in molecular docking. Proteins. 2010a; 78: 1503-1519.
25. Mashiach E, Nussinov R, Wolfson HJ. FiberDock: a web server for flexible induced-fit backbone refinement in molecular docking. Nucleic Acids Res. 2010b; 38: W457-461.
26. Dundas J, Ouyang Z, Tseng J, Binkowski A, Turpaz Y, *et al*. CASTp: computed atlas of surface topography of proteins with structural and topographical mapping of functionally annotated residues. Nucleic Acids Res. 2006; 34: W116-118.
27. Serrano SM, Jia LG, Wang D, Shannon JD, Fox JW. Function of the cysteine-rich domain of the haemorrhagic metalloproteinase atrolysin A: targeting adhesion proteins collagen I and von Willebrand factor. Biochem. J. 2005; 391: 69-76.
28. Serrano SM, Kim J, Wang D, Dragulev B, Shannon JD, *et al*. The cysteine-rich domain of snake venom metalloproteinases is a ligand for von Willebrand factor A domains: role in substrate targeting. J. Biol. Chem. 2006; 281: 39746-39756.
29. Serrano SM, Wang D, Shannon JD, Pinto AF, Polanowska-Grabowska RK, *et al*. Interaction of the cysteine-rich domain of snake venom metalloproteinases with the A1 domain of von Willebrand factor promotes site-specific proteolysis of von Willebrand factor and inhibition of von Willebrand factor-mediated platelet aggregation. FEBS J. 2007; 274: 3611-3621.
30. Tanjoni I, Evangelista K, Della-Casa MS, Butera D, Magalhães GS, *et al*. Different

regions of the class P-III snake venom metalloproteinase jararhagin are involved in binding to α2β1integrin and collagen. Toxicon. 2010; 55: 1093-1099.

31. Hudson BG, Reeders ST, Tryggvason K. Type IV collagen: structure, gene organization, and role in human diseases. Molecular basis of Goodpasture and Alport syndromes and diffuse leiomyomatosis. J. Biol. Chem. 1993; 268: 26033-26036.
32. Farach-Carson MC, Carson DD. Perlecan--a multifunctional extracellular proteoglycan scaffold. Glycobiology. 2007; 17: 897-905.
33. Iozzo RV. Basement membrane proteoglycans: from cellar to ceiling. Nat. Rev. Mol. Cell. Biol. 2005; 6: 646-656.
34. Paes-Leme AF, Escalante T, Pereira JG, Oliveira AK, Sanchez EF, *et al*. High resolution analysis of snake venom metalloproteinase (SVMP) peptide bond cleavage specificity using proteome based peptide libraries and mass spectrometry. J. Proteomics. 2011; 74: 401-410.
35. Manka SW, Carafoli F, Visse R, Bihan D, Raynal N, *et al*. Structural insights into triple-helical collagen cleavage by matrix metalloproteinase 1. Proc. Natl. Acad. Sci. U S A. 2012; 109: 12461-12466.
36. Baramova EN, Shannon JD, Bjarnason JB, Fox JW. Identification of the cleavage sites by a hemorrhagic metalloproteinase in type IV collagen. Matrix. 1990; 10: 91-97.
37. Sundaramoorthy M, Meiyappan M, Todd P, Hudson BG. Crystal structure of NC1 domains. Structural basis for type IV collagen assembly in basement membranes. J. Biol. Chem. 2002; 277: 31142-31153.
38. Yurchenco PD, Amenta PS, Patton BL. Basement membrane assembly, stability and activities observed through a developmental lens. Matrix Biol. 2004; 22: 521-538.

Supplementary Material

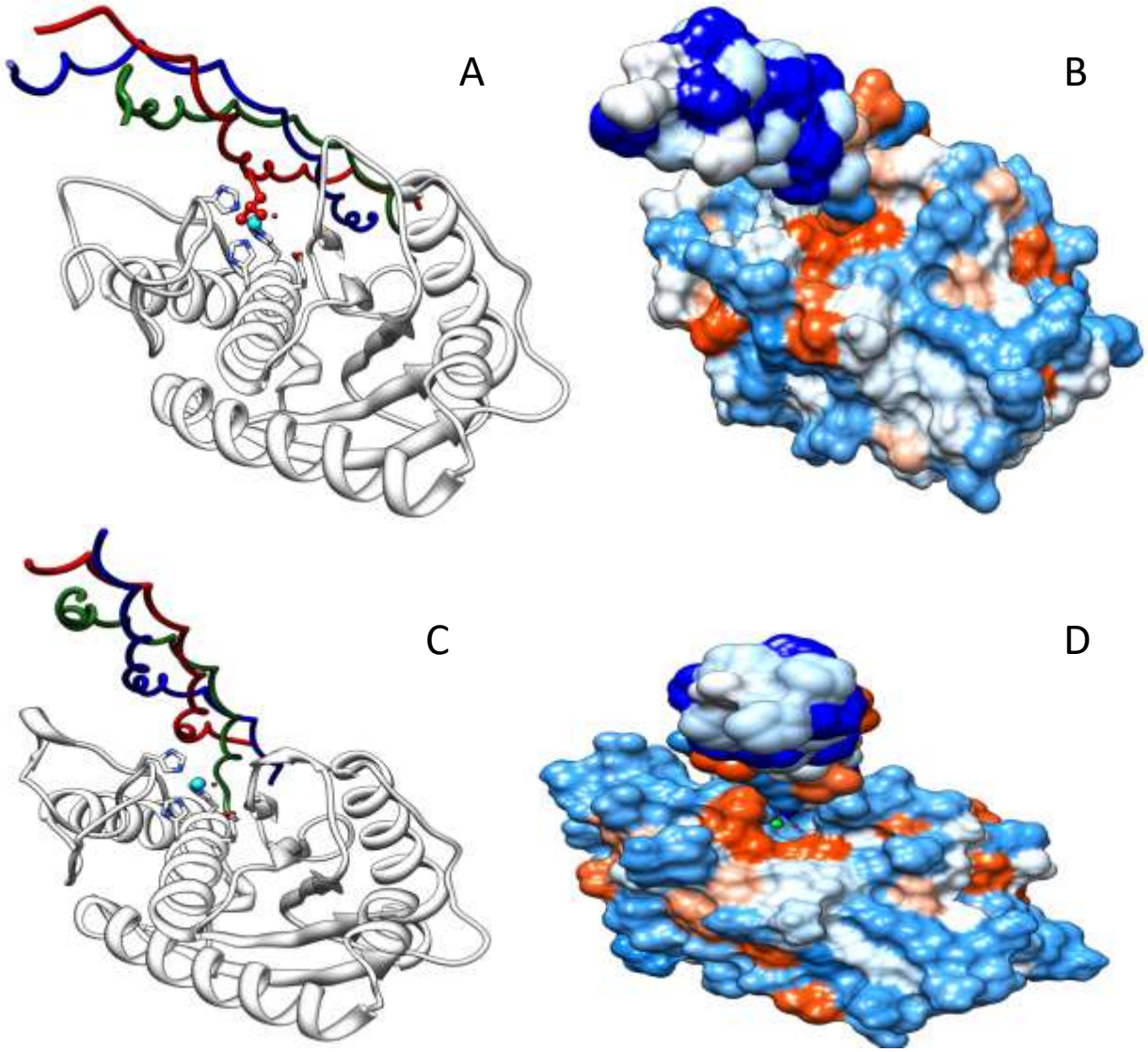

Figure 1. Interaction of hemorrhagic and non-hemorrhagic P-I SVMPs and triple-helical region of collagen. **A.** Ribbon representation of the interaction of Acutolysin A with triple-helical collagen. **B.** Hydrophobicity-surface representation of the interaction between Acutolysin A and triple-helical type IV collagen. Note in B that active site is filled by collagen chains. **C.** Ribbon representation of the interaction of H2-proteinase with triple-helical collagen. **D.** Hydrophobicity-surface representation of the interaction between H2-proteinase and triple-helical collagen. Note in **D** that the active site is not occupied by collagen chains. In **A** and **C**, the catalytic water and the active site of SVMPs are displayed in sticks, and Zn^{2+} ion is colored in cyan. The chains A, B and C of collagen are colored in red, green and blue, respectively. The Leu residue occupying the active site cleft of Acutolysin A is shown in balls and sticks.

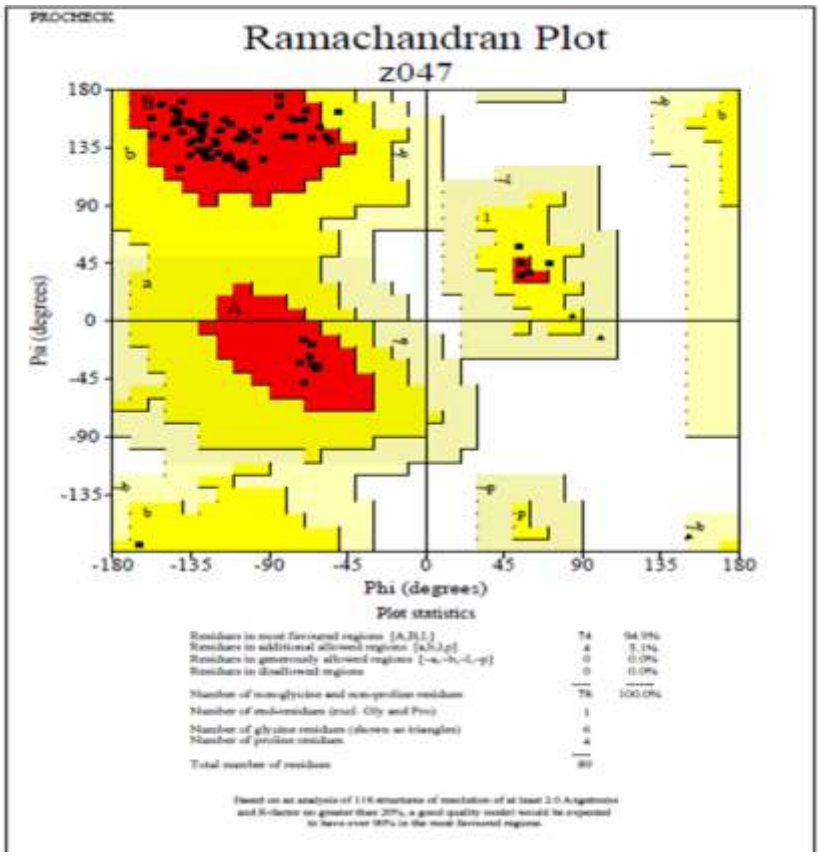

Figure 2. The Ramachandran plot of modeled IG3 domain of perlecan. The favored and most favored region are shown red and brown, respectively, yellow is the generally allowed, and pale yellow corresponds to disallowed regions.

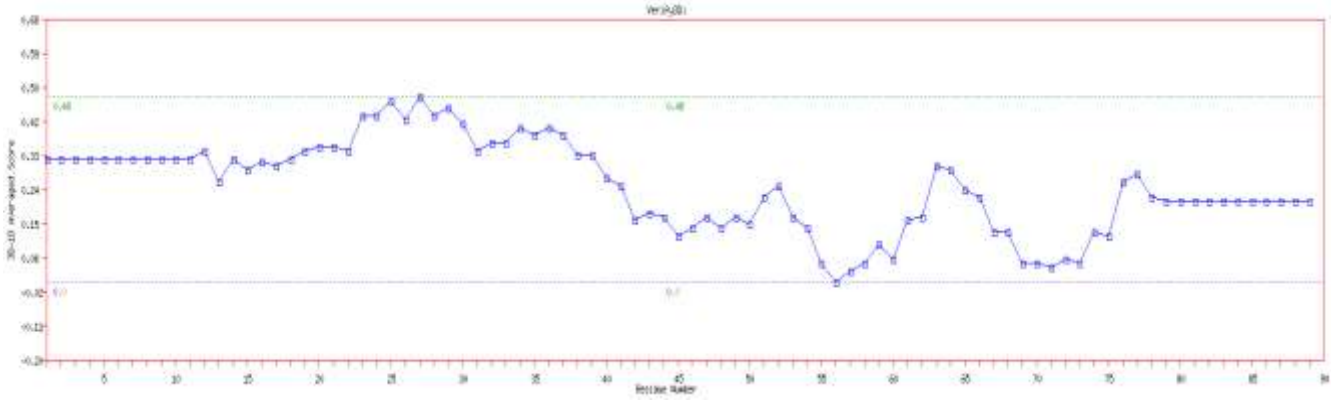

Figure 3. Verify-3D analysis. Positive scores suggest that the residues are compatible with their environments in the model build for IG3 domain of perlecan. The lowest and highest values are shown.

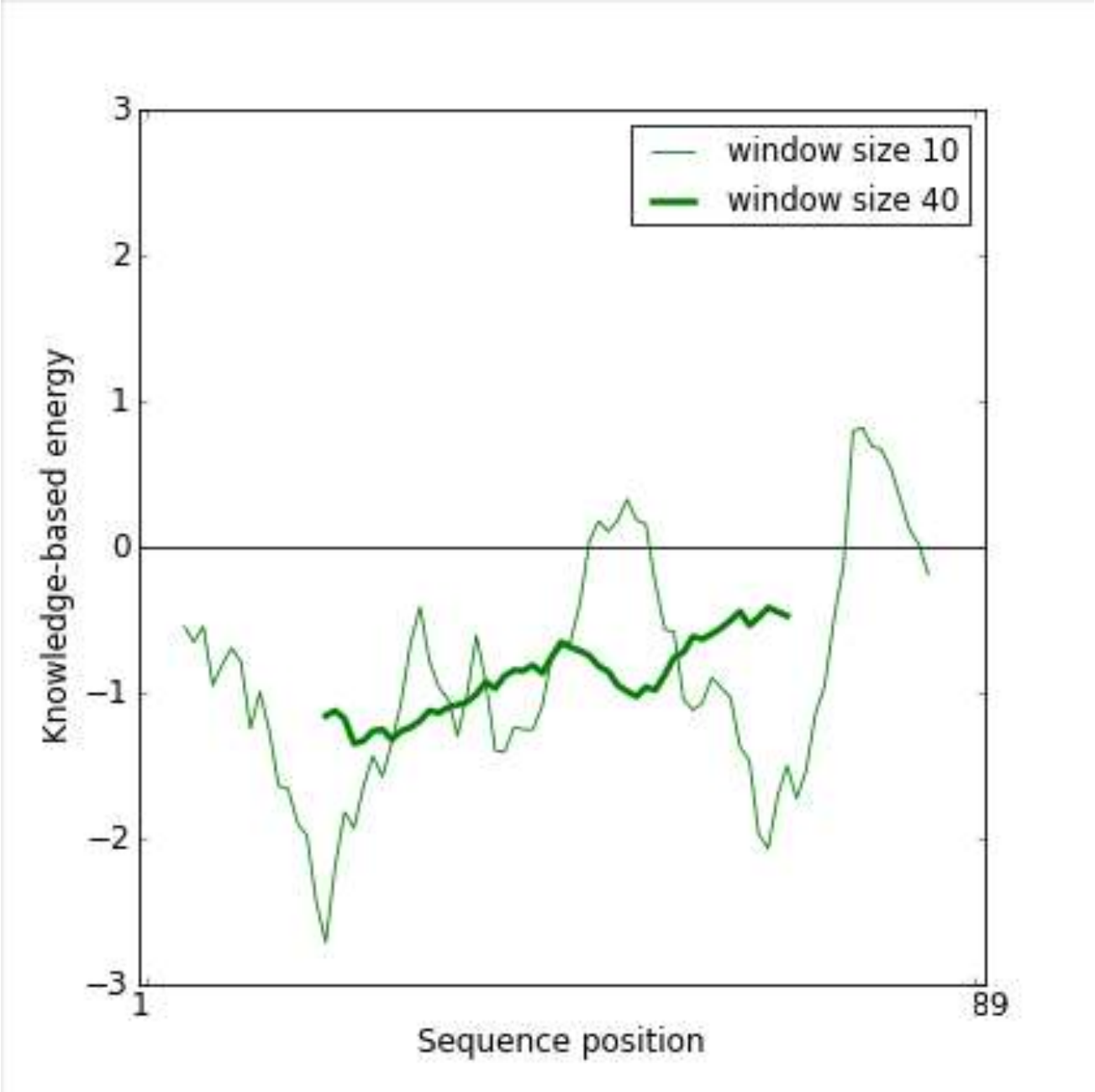

Figure 4. ProSA energy plot calculated for the IG3 domain of perlecan homology model. The energy plot displayed by ProSA shows the local model quality by plotting energies in function of the amino acid sequence position. Positive values correspond to problematic or erroneous parts of a model. When the fragment of 10 residues was evaluated, most of them were in the negative region. However, when a fragment of 40 residues was evaluated, none of the residues is outside the negative region.

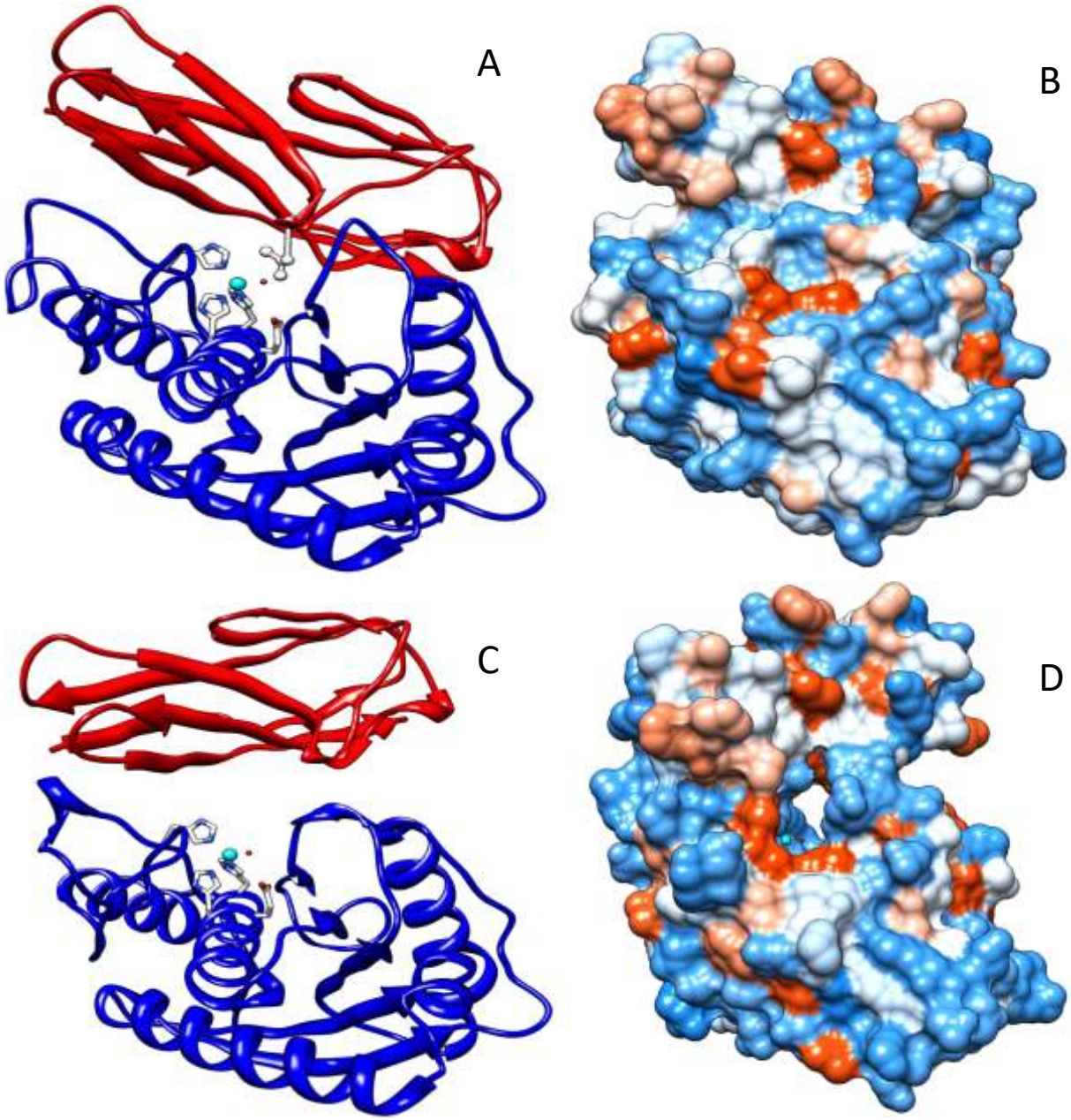

Figure 5. Docking results between hemorrhagic and non-hemorrhagic P-I SVMPs and IG3-domain of perlecan. **A.** Ribbon representation of the interaction of Acutolysin A with IG3-domain of perlecan. B**.** Hydrophobicity-surface representation of the interaction between Acutolysin A and IG3-domain of perlecan. **C.** Ribbon representation of the interaction of H2-proteinase with IG3-domain of perlecan. **D.** Hydrophobicity-surface representation of the interaction between H2-proteinase and IG3-domain of perlecan. In **A** and **C**, the catalytic water and the active site of SVMPs are displayed in sticks, and Zn^{2+} ion is colored in cyan. SVMPs and IG3-domain of perlecan are colored in blue and red, respectively. In **A**, the Leu residue occupying the active site cleft of Acutolysin A is shown in balls and sticks. Note in **B** that the substrate binding pocket is occupied by IG3-domain of perlecan, whereas in **D** the substrate binding pocket is unfilled.

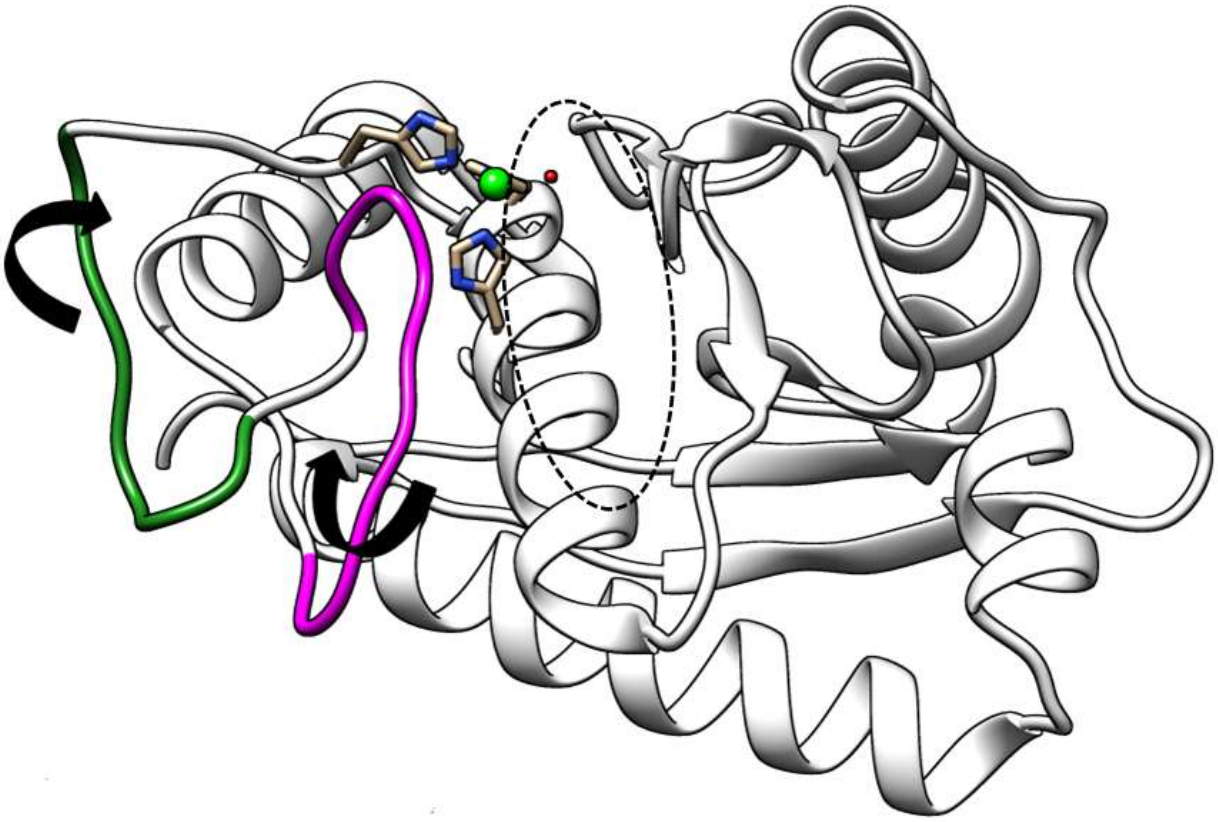

Figure 6. Ribbon representation of BaP1. The loop that is flexible in hemorrhagic PI SVMPs is shown in green (residues 156-165), whereas the one that is flexible in the non-hemorrhagic PI-SVMPs is shown in magenta (residues 167-175). Green and red spheres represent the zinc ion and catalytic water, respectively. Arrows represent directions of the possible movements of the loops. The dotted ellipse indicates the peptide binding pocket.

